CrossMark

Original Research

Microstructure-modified biodegradable magnesium alloy for promoting cytocompatibility and wound healing in vitro

Da-Jun Lin[1] · Fei-Yi Hung[1] · Ming-Long Yeh[2] · Truan-Sheng Lui[1]

Abstract The microstructure of biomedical magnesium alloys has great influence on anti-corrosion performance and biocompatibility. In practical application and for the purpose of microstructure modification, heat treatments were chosen to provide widely varying microstructures. The aim of the present work was to investigate the influence of the microstructural parameters of an Al-free Mg–Zn–Zr alloy (ZK60), and the corresponding heat-treatment-modified microstructures on the resultant corrosion resistance and biological performance. Significant enhancement in corrosion resistance was obtained in Al-free Mg–Zn–Zr alloy (ZK60) through 400 °C solid-solution heat treatment. It was found that the optimal condition of solid-solution treatment homogenized the matrix and eliminated internal defects; after which, the problem of unfavorable corrosion behavior was improved. Further, it was also found that the Mg ion-release concentration from the modified ZK60 significantly induced the cellular activity of fibroblast cells, revealing in high viability value and migration ability. The experimental evidence suggests that this system can further accelerate wound healing. From the perspective of specific biomedical applications, this research result suggests that the heat treatment should be applied in order to improve the biological performance.

✉ Fei-Yi Hung
  fyhung@mail.ncku.edu.tw

[1] Department of Materials Science and Engineering, National Cheng Kung University, Tainan 701, Taiwan

[2] Department of Biomedical Engineering, National Cheng Kung University, Tainan 701, Taiwan

1 Introduction

Magnesium-based materials are attracting much attention for biomedical applications because their degradation products can be bio-safely absorbed or excreted [1, 2]. Nowadays, many new toxicity-free magnesium alloy systems are being developed for medical devices, especially the Mg–Zn, Mg–Ca series [3–5], which combine good mechanical strength with satisfactory biocompatibility. Thus, the developed bio-Mg materials can be considered a new choice for orthopedic [1], cardiovascular [6] or suture materials [7]. However, the applicability limitation for magnesium materials is the unfavorable corrosion resistance. It is widely recognized that the insufficient corrosion resistance of magnesium implants will diminish the strength retention and encounter the problem of early-failure during the implantation period [8]. Therefore, it is necessary that magnesium materials be modified by proper post process to enhance the corrosion resistance, thereby further promoting such materials' bio-applicability.

It has been reported that the mechanical properties and the anti-corrosion performance of magnesium alloys and other engineered alloys depend strongly on the final microstructural features [5, 9]. Recent studies have pointed out that applying proper heat treatment can eliminate internal defects and residual stress for achieving an optimal microstructure [10, 11]. Heat treatment of magnesium alloys effectively modifies the corrosion mechanism and enhances corrosion resistance against corrosive media [5]. Accordingly, the degradation property and ion release rate can be controlled. In ideal conditions, degradation products (Mg^{2+} ions) can be gradually reused as required mineral nutrients for body supplement. Several studies have investigated the effects of Mg ions on in vitro cell behavior, and reported the Mg ion-induced promoting effect on

🖄 Springer

the proliferation rate of osteoblasts, endothelial cells and fibroblasts [12–14]. Furthermore, Mg and other biocompatible metal ions (e.g.: Zn, Mn, etc.) play an important role in protein synthesis, enzyme construction and the maintenance of basic metabolism [15–17]. It can be reasonably predicted that well heat-treated Mg alloys can improve functionality, including better corrosion resistance and biocompatibility. So far, only few reports have focused on the biological properties of heat treatment-modified Mg alloys.

In the present study, the microstructure of aluminum-free Mg–Zn–Zr alloy (ZK60) was modified by heat treatment. Different solution-treatment temperatures were applied to investigate the performance of specific microstructure features, and to determine the optimum solution-treatment conditions of ZK60. In addition, the electrochemical corrosion properties and cytocompatibility were also studied. To realize the bio-functionality of the optimal microstructure, attention is particularly focused on the Mg-ion release affecting the wound healing efficiency of fibroblasts. The related outcomes are expected to verify the potential of microstructure-modified ZK60 for specific biomedical applications, such as high strength bone implants or degradable suture wire.

2 Materials and methods

2.1 Materials preparation and microstructure characterization

Extruded ZK60 magnesium alloy (5.48 wt% Zn, 0.42 wt% Zr) was used in this study, and processed into a circular plate (12 mm in diameter).The as-extruded alloy was named as the ZK60-F specimen. Two solution treatments (T4) of the alloy were carried out, one at 400 °C and the other at 500 °C, for 2 h in a tubular vacuum furnace, followed by water quenching at room temperature. The names of the solution heat-treated samples were assigned according to heating temperature, hereafter referred to as H400 and H500, respectively.

For microstructure characterization, all three ZK60 samples (ZK60-F, H400 and H500) were ground and polished to 0.05 μm and finally etched by picric-acetic solution (80 mL ethanol, 10 mL acetic acid, 15 g picric acid powder, purchased from Panreac (Spain)). Optical microscopy (BX41M-LED, Olympus) and environmental scanning electron microscopy (Quanta 400-FEG, FEI) with an energy dispersive spectrometer (EDAX) were used for microstructure characterization. Grain size was determined by the linear intercept method according to the ASTM E112-96 standard. With the aim to realize the effects of grain size and solute atom on heat treated ZK60, micro-

hardness measurement (HMV-2000L, Shimadzu) was performed on the polished surface of the ZK60-F, H400 and H500 specimens. The loaded force was 100 g and the holding time was 10 s. The constituent phases were characterized by X-ray diffraction (XRD, D8 Discover, Burker) with Cu Kα radiation, from which diffraction patterns were obtained between the 2θ values of 20°–80°.

2.2 Electrochemical corrosion test

The ZK60-F, H400 and H500 specimens for the electrochemical corrosion test were embedded in an epoxy resin. The exposed area of the sample surface to the solution was controlled within 1 cm^2. A standard three-electrode electrochemical cell was used for the electrochemical polarization test with a platinum plate as the counter electrode and a saturated calomel electrode (SCE) as the reference electrode. The experimental environment was fixed at 37 °C in a beaker containing 350 mL of revised simulated body fluid (r-SBF) solution. The composition of the r-SBF (per liter, dissolved in de-ionized water) was as follows: 5.403 g NaCl, 0.736 g NaHCO$_3$, 2.036 g Na$_2$CO$_3$, 0.225 g KCl, 0.182 g K$_2$HPO$_4$, 0.310 g MgCl$_2$·6H$_2$O, 11.928 g HEPES, 0.293 g CaCl$_2$ and 0.072 g Na$_2$SO$_4$. It was buffered to pH 7.4 at 37 °C by adding NaOH. The polarization test used a PARSTAT 2273 electrochemistry workstation with a scanning rate of 1 mV/s from −2.0 to −1.0 V.

To observe the corrosion morphology, the experimental samples were treated with a cleaning process after the polarization test. The samples were rinsed with distilled water and immersed with chromic acid/silver nitrate solution (200 g/L CrO$_3$ + 10 g/L AgNO$_3$) to remove the corrosion products.

2.3 Hydrogen evolution test

Hydrogen evolution tests were employed to realize the corrosion tendencies in different solutions containing r-SBF and cell culture medium (DMEM + 10 %FBS). In the experimental setup, a burette with a funnel head was placed over the specimen. A dosing pump was connected to the burette by silicon tube and control valve, which ensured the same initiation condition for each test. The experimental environment was fixed at 37 °C in a water bath and the solution volume to surface area ratio was fixed at 100 mL/cm^2.

2.4 Cell culture and cytotoxicity test

Mouse embryo fibroblast cells (NIH-3T3, ATCC® CRL-1658™) were used to exam the cytocompatibility of ZK60 and its modified microstructures. Cells were grown in Dulbecco's Modified Eagle's Medium (DMEM) (Gibco, USA) with high glucose, supplemented with 10 % fetal bovine

serum (FBS) and 1 % antibiotics, and were cultured in a 5 % CO_2 incubator at 37 °C under a humidified atmosphere.

Cytotoxicity tests were performed by the indirect method, and the extracts prepared according to ISO 10993-5 [18]. Some extracts were collected and diluted manually, and then analyzed for their Mg content by atomic absorption spectroscopy (AAS, PerkinElemer). For the cell viability test, cells were cultured in 96-well plates at 5×10^3 cells/100 μL of medium in each well and incubated for 24 h to allow initial cell adhesion. The medium was then replaced with 100 μL of experimental extract. After incubating the cells for 1, 3 and 6 days, respectively, a CellTiter96-kit (Promega, USA) was used to test the viability rate. The absorbance of the CellTiter96-treated solution was measured by ELISA reader at a wavelength of 490 nm. The acquired absorbance values form the ELISA reader were recalculated to obtain the cell viability (%) according to the following formula:

$$
\begin{aligned}
\text{Cell viability } (\%) = &\left[(OD_{test} - OD_{blank}) \right. \\
&\left. \big/ (OD_{negative} - OD_{blank}) \right] \times 100\%
\end{aligned}
\tag{1}
$$

Cell viability measurements were given as a mean value ± standard deviation (n = 5), and an analysis of one-way variance (ANOVA) was conducted to evaluate the statistical significance of differences. Difference at $P \leq 0.05$ was considered to be statistically significant.

2.5 Wound healing assay

Wound healing was evaluated by using the Culture-Inserts system (Ibidi, München, Germany). NIH-3T3 cells (2×10^4 cells/80 μL of medium) were seeded and cultured in culture medium for 12 h to allow initial cell adhesion. Then, the culture inserts were removed and replaced with experimental extracts, leaving a 500 μm cell-free wound. Cells were continuously cultured at 37 °C in the experimental extracts (negative control and H400) to characterize the bio-functionality of the microstructure-modified ZK60. Photographs of the in vitro wounds were taken at 0, 6 and 24 h with an optical microscope, the experiments of which were performed in triplicate. After acquiring the experimental photos, the wound closure percentages were calculated by ImageJ software (NIH, USA).

3 Results and discussion

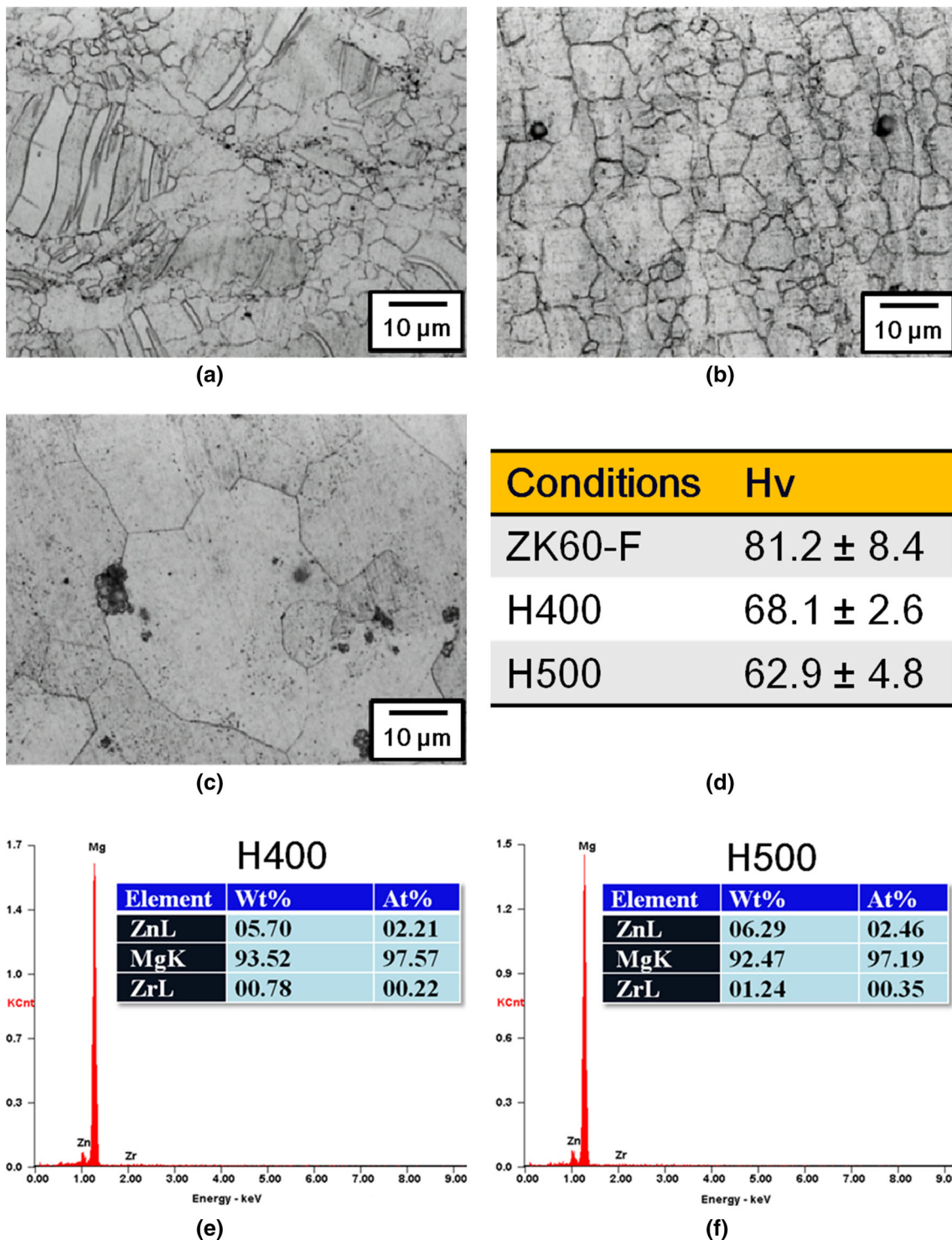## 3.1 Microstructural characteristics

The microstructures of all specimens are shown in Fig. 1. The ZK60-F specimen shows a typical extrusion feature:

many fine dynamic recrystallization (DRX) grains were observed in the matrix. However, there existed some non-uniform regions with many twins inside the coarse grains, as shown in Fig. 1a. Figure 1b illustrates the microstructure of the H400, and reveals that the fully recovered matrix had equiaxed grains with an average grain size of 8.6 μm. The solution treatment successfully eliminated deformation twins and softened the matrix, which was reflected in the reduction in hardness value (see Fig. 1d), where the hardness of H400 was much lower than that of ZK60-F. According to the above results, it can be confirmed that the solution temperature at 400 °C can reduce the defects and simultaneously homogenize the microstructure of ZK60.With a further increase of the treatment temperature to 500 °C (H500), grain growth was found to measure ∼36 μm (Fig. 1c); as such, the temperature variation did significantly alter the grain size as compared with the H400 specimen (∼4 times bigger than H400).The hardness of H500 decreased to Hv62.9, due to its matrix having the lowest grain boundary density.

Figure 2 shows the XRD patterns of the experimental specimens. The pattern of the ZK60-F confirms the coexistence of the $MgZn_2$ crystalline signal, which is the major secondary phase in Mg-Zn alloy. After solution-heat treatment, the signal of $MgZn_2$ disappeared. Furthermore, the major peaks, such as (100), (002) and (101) of α-Mg exhibited a slight 0.2° red-shift, the intensity of which changed with increasing solution temperature. To investigate further, the grains' interior composition was measured by EDS analysis to better understand the relationship between the solute atoms (solid-soluted Zn and Zr) and solution temperature. According to the Mg–Zn binary phase diagram [19], the maximum solubility of Zn in α-Mg is 6.2 wt% (i.e. 2.5 at.%). As shown in Fig. 1e, there exists a great amount of solute-Zn atoms (5.7 wt%) in the H400 matrix; accordingly, increasing the process temperature to 500 °C can further reach the theoretical saturation value (6.29 wt%). This is because the constituent phases dissolved and the diffusion rate of Zn and Zr in the matrix increased. With the dissolution of the $MgZn_2$ phase, the element composition distribution of H400 and H500 appeared more even than that of ZK60-F. Clearly, solution-heat treatment can significantly affect the metallography, crystallinty and hardness. Moreover, the effects of recovery and recrystallization are the critical influential mechanisms in the presented modified-ZK60, showing a great influence of originally existing defects (twins and stored internal energy induced by extrusion) on materials properties.

3.2 In vitro corrosion behavior

In order to achieve a desired level of practical properties, the microstructure correlation with corrosion behavior can

(a)

(b)

(c)

Conditions	Hv
ZK60-F	81.2 ± 8.4
H400	68.1 ± 2.6
H500	62.9 ± 4.8

(d)

Element	Wt%	At%
ZnL	05.70	02.21
MgK	93.52	97.57
ZrL	00.78	00.22

(e)

Element	Wt%	At%
ZnL	06.29	02.46
MgK	92.47	97.19
ZrL	01.24	00.35

(f)

Fig. 1 Typical microstructures of each group: a ZK60-F, b H400, and c H500. d Corresponding Vickers hardness of each group (data presented as mean ± SD, n = 3.). EDS analyses for e H400 and f H500

be very useful for planning the modification process. The electrochemical corrosion test is a conventional method that can estimate the in vitro anti-corrosion performance of different microstructural features [20]. In the present study, a three-electrode testing system was employed to measure the polarization corrosion curve, the results of which are shown in Fig. 3 and Table 1. As can be seen, the polarization curves of the three experimental groups show
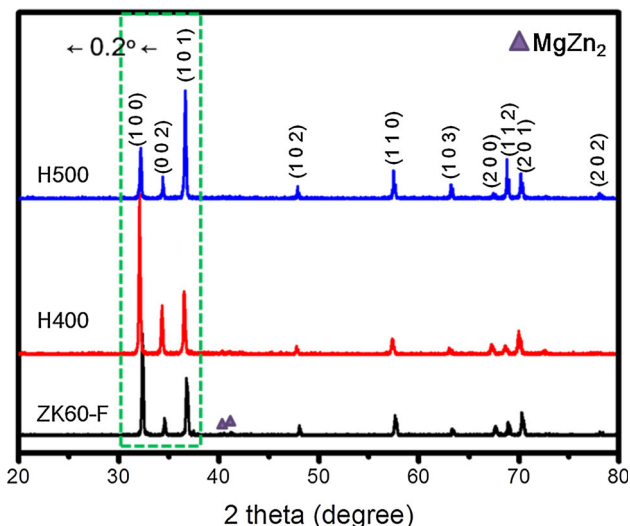
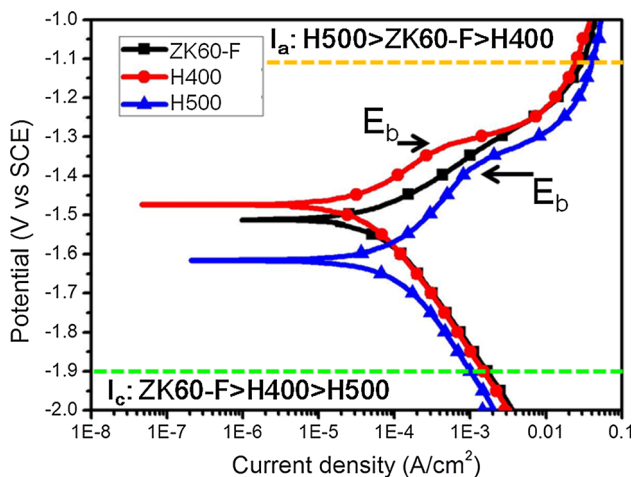Fig. 2 XRD patterns of ZK60-F, H400 and H500

Fig. 3 Potentiodynamic polarization curves obtained in r-SBF solution at 37 °C. The experiment was repeated twice with similar outcome

different electrochemical behaviors. In general, the cathodic current density is proportional to the amount of secondary phase in the matrix [21]. After solution-heat treatment, the secondary phases decomposed and were absorbed into the grain, resulting in the detected solute atoms by EDS analysis (Figs. 1e, f). Hence, the H400 and H500 specimens show a relatively lower cathodic current density than ZK60-F. Moreover, the effect of the heat

treatment also affected the Tafel corrosion region, which modified the corrosion current density. The corrosion current density of the three experimental groups constituted the following order: H400 (37 μA/cm²) < ZK60-F (64 μA/cm²) < H500 (126 μA/cm²). According to the following equation of polarization resistance (Eq. 2) [22], a relatively lower I_{corr} indicates better anticorrosion performance.

$$R_p = \frac{\beta_a \beta_c}{2.303(\beta_a + \beta_c)I_{corr}} \qquad (2)$$

R_p: polarization resistance, β_a: anodic slope, β_c: cathodic slope, I_{corr}: corrosion current.
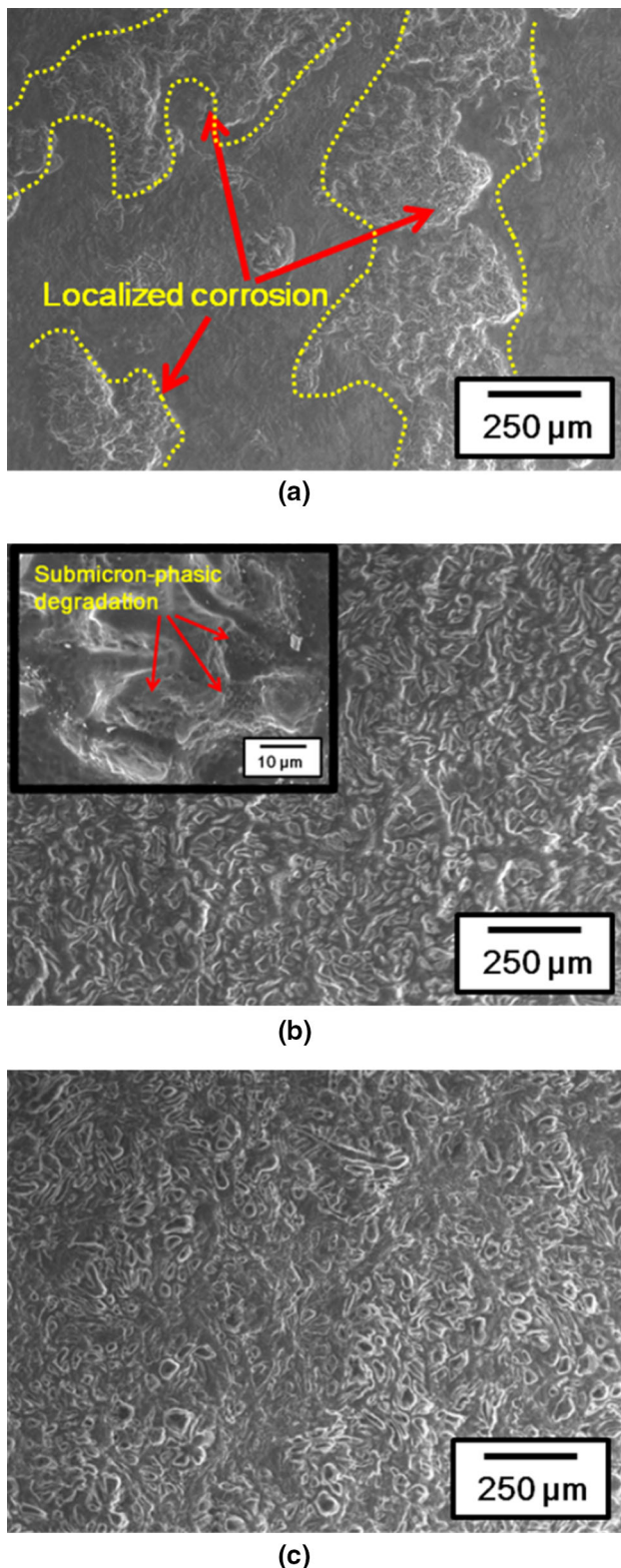
The electrochemical corrosion rate (CR) of the experimental groups obtained from the corrosion current density was calculated according to the following reported equation (Eq. 3) [23]:

$$CR = 22.85 * I_{corr} \qquad (3)$$

According to the analysis of the H400 and H500 anode polarization curves, a significant change of current slope suggests that both microstructures had the passivation behavior, indicating the formation of a protective oxide layer on the surface. In particular, H400 had the highest corrosion resistance, lowest anodic current density and showed the passivation behavior, implying that its microstructure can effectively protect against corrosion from the simulated biological environment [24]. Recent studies have also revealed the influence of the alloying system and microstructure on the corrosion of magnesium alloys. Cheng et al. reported that the electrochemical corrosion resistance of ZK60 is higher than other commercial magnesium alloys, such as AZ31, AZ91 and AM60 [25]. NaingNaing Aung et al. proposed that the deformation twins and grain size affected the corrosion rate and corrosion behavior, where corrosion was particularly enhanced in twins-containing magnesium matrix [11]. In the present study, ZK60-F showed a bimodal microstructure, wherein the twins exist in coarse grains. The non-uniform microstructure could not stabilize the surface oxide layer to prevent corrosion propagation to certain areas (Fig. 4a), resulting in a non-passivated anode polarization curve and localized corrosion morphology. As shown in Fig. 4b, c, the deleterious effects of twins and the bimodal microstructure were modified in the H400 and H500 matrixes, in which a twin-free and uniform microstructure demonstrates the homogenous submicron-

	E_{corr} (V)	I_{corr} (A/cm²)	β_c (mV/dec)	β_a (mV/dec)	R_p (Ω-cm²)	CR (mm/year)
ZK60-F	−1.51	6.48×10^{-5}	273	135	605	1.48
H400	−1.43	3.70×10^{-5}	308	139	1123	0.84
H500	−1.61	1.26×10^{-4}	312	269	497	2.88

Table 1 The electrochemical polarization properties of ZK60-F, H400 and H500

(a)

(b)

(c)

Fig. 4 Corrosion morphologies of polarization-tested specimens **a** ZK60-F, **b** H400, and **c** H500

phasic degradation behavior for designing modified-microstructures to achieve an ideal biodegradation model. However, the solid-solution temperature should be precisely controlled to prevent grain growth, which could lead to a lower corrosion resistance. The relatively lower density of the grain boundaries also means a lower physical barrier in the matrix, which suggests a higher oxidation probability and unfavorable corrosion resistance for H500.

Figure 5 shows the hydrogen evolution results of ZK60-F, H400 and H500 in the r-SBF and culture medium (DMEM + 10 %FBS) solutions measured at 37 °C. The hydrogen evolution volume of the different corrosive mediums (r-SBF and culture medium) indicate the same tendency; however, it can be seen that all of the culture media examined samples have lower hydrogen evolution volumes than that of the r-SBF. This might be due to the effect of the FBS, permitting more proteins and organic compounds to be absorbed on the magnesium surface, and further reduce its corrosion reaction. Liu et al. also found that corrosion was inhibited when the magnesium surface was covered with proteins or biological organic compounds [26]. Among the three different microstructures of the ZK60 specimens, H400 exhibited the lowest hydrogen evolution volume during the testing period, whereas H500 showed the highest. The volume of evolved hydrogen gas can be correlated to the corrosion rate. The hydrogen evolution amount for the three groups from low to high is: H400 < ZK60-F < H500. The same trend was obtained from the electrochemical test, which showed that the corrosion resistance of H400 was much higher than those of the other two groups. The electrochemical and hydrogen evolution tests indicated that there is an important anti-corrosion performance difference in the configuration of microstructures between ZK60-F, H400 and H500. Both of the in vitro corrosion results demonstrate the considerable potential of H400 for applications in bio-degradable material.

3.3 In vitro biological behavior of different microstructures

Figure 6 shows the NIH-3T3 cell viability of cells cultured in the extraction medium for 1, 3, and 6 days. Results of the cell cytotoxicity test show that all examined microstructures of ZK60 were cytotoxic-free according to ISO 10993-5:1999 (Grade 1: higher than 75 %). Interestingly, it was found that only the extract of H400 increased NIH-3T3 growth. The difference in viability value between H400 and the other two experimental extracts (ZK60-F and H500) at day 1 were confirmed statistically ($P < 0.05$),

Fig. 5 The lab-made equipment for the hydrogen evolution test and the hydrogen evolution curves of ZK60-F, H400 and H500 at 37 °C The experiment was repeated twice with similar outcome
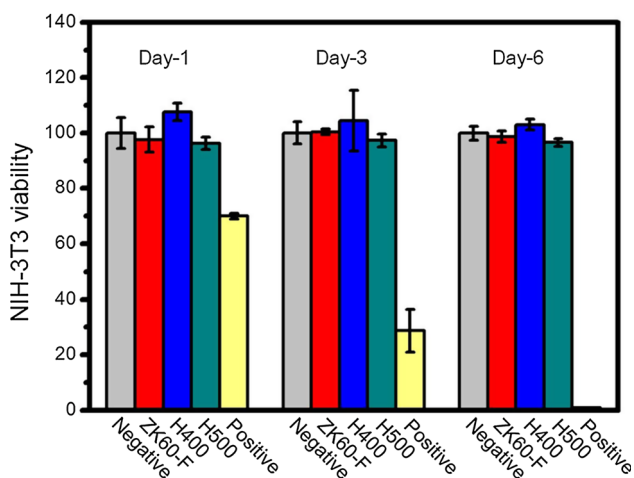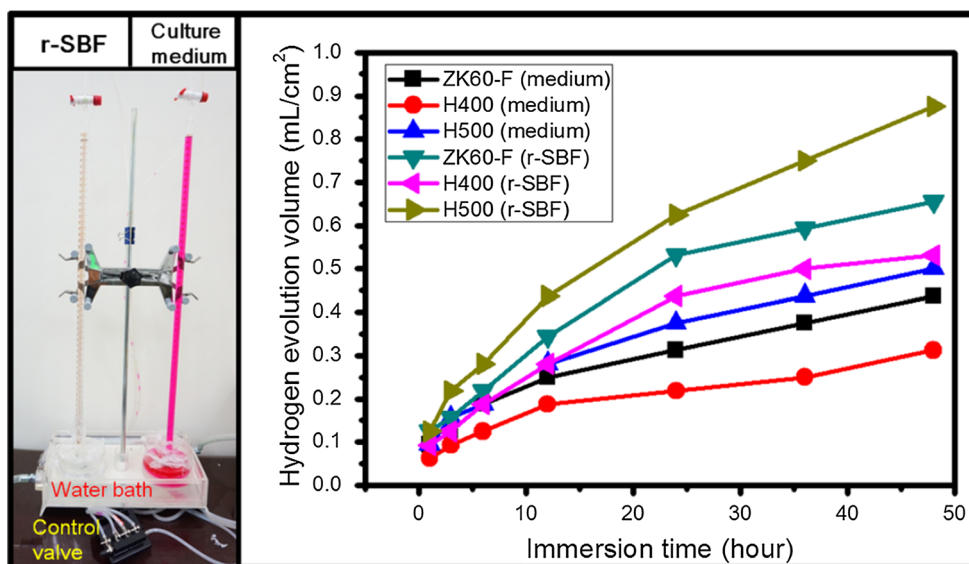
Fig. 6 Cell viability of NIH-3T3 cells after 1, 3 and 6 days incubation (data presented as mean ± SD, n = 5)

which indicates that the H400 can enhance the cellular proliferation in the early stage. In comparing the results of cell viability and corrosion, it can be reasonably assumed that the released Mg ions of H400 provided the most suitable environment for NIH-3T3 cells. To further investigate the exact value of ion concentration, AAS analysis was performed to measure the magnesium content, which indicated that 13.2 mM of magnesium existed in the H400 extract.

In previous reports, magnesium ions were found to participate in a massive amount of biochemical processes, including signaling molecules activation [16], DNA synthesis, RNA transcription [15], regulation of cell cycle [27], stabilization of cell membranes and collagen
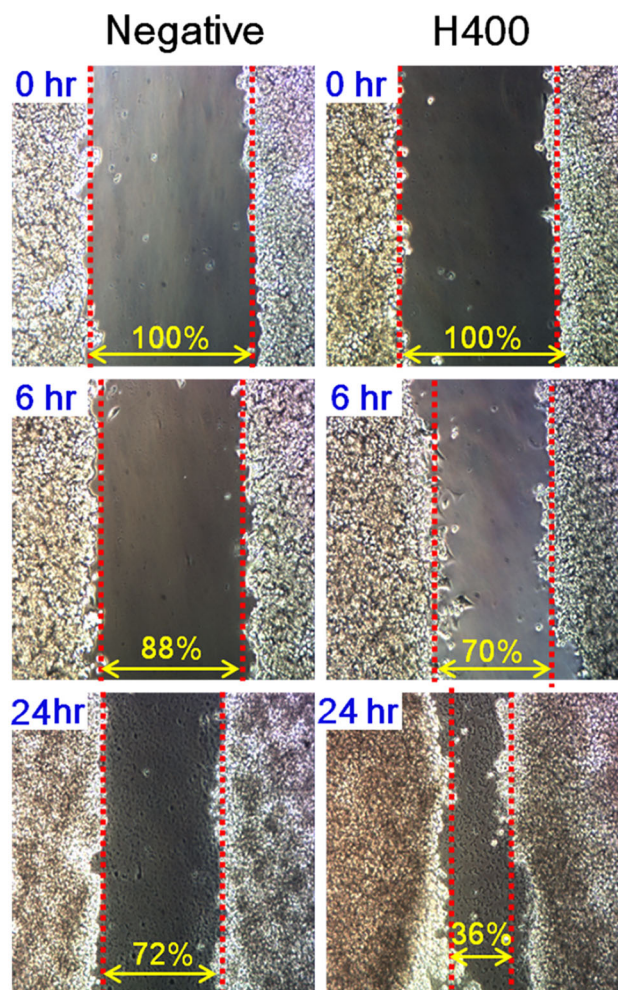
Fig. 7 Wound healing results for negative control and H400 at t = 0, 6 and 24 h

Fig. 8 Schematic representation of the wound healing promotion mechanism
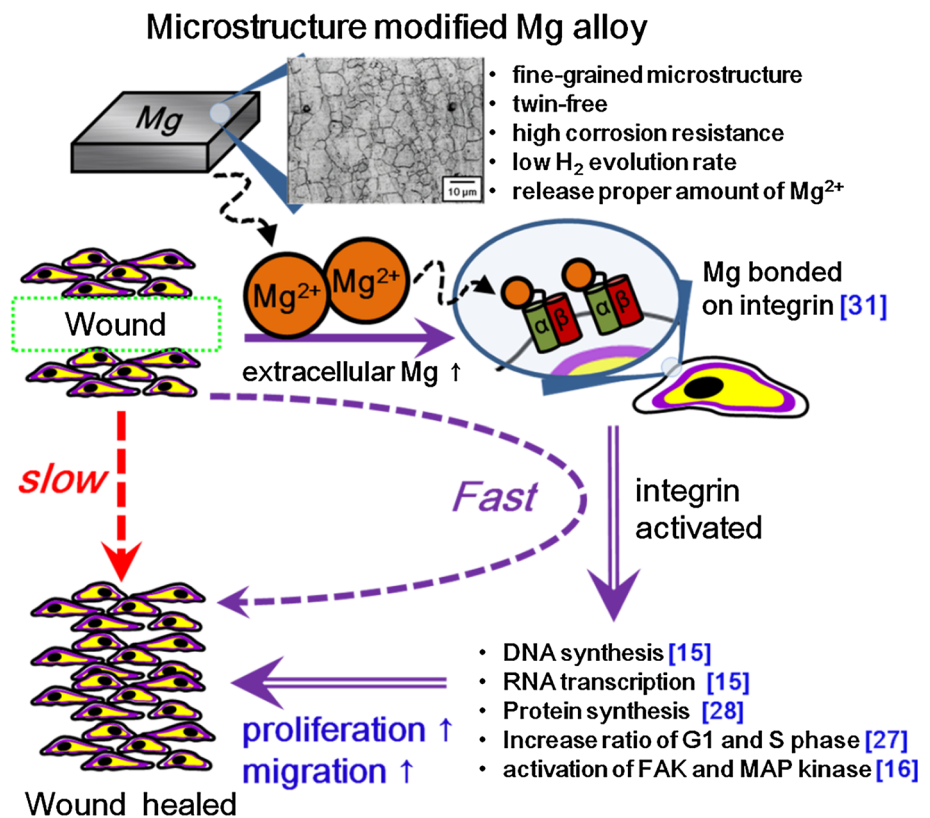
synthesis [28]. Therefore, dosing a acceptable level of concentration of extracellular magnesium ions can effectively enhance cell activity. According to the above results, H400 was certified as the most reliable microstructure of ZK60 (with the highest corrosion resistance and cell viability). To measure cell migration, NIH-3T3 cells were seeded into the cavities of ibidi molds. Hence, a simulated wound (at the cellular level) was created in the middle of the cell sheets, after which the cells were incubated with the control and H400 extract in order to investigate the wound healing performance. After 24 h observation, NIH-3T3 showed a 64 % wound closure for H400. In contrast, the negative control showed only a 28 % wound closure. Previously, Zhao et al. added 10–20 mM of magnesium salts into the culture medium, which enhanced the viability, proliferation and gene expression of human coronary artery endothelial cells (HCAECs) [29]. Lange et al. revealed that divalent ions can regulate the integrins on cell membranes, and further verified the effect of extracellular magnesium concentration on cell proliferation, differentiation and migration ability [30]. Furthermore, Grzesiak et al. reported that Mg^{2+} ions bind on the α-intergrin through EF-hand, playing a direct role in accelerating cell adhesion and migration [31]. Moreover, Mg is widely acknowledged as being involved in cell cycle regulation. Rubin et al. described the relationship between the sequence of cellular

physiology and the availability of Mg [32]. The observations provided the preliminary input for modeling the contribution of Mg in the different phases of the cell cycle. Most importantly, an insufficient Mg environment may cause cell growth arrest, resulting in an increased percentage of cells in the G0-phase and a decreased percentage in the S-phase [27]. On the other hand, Hazelton et al. described the ability of cells to enter the S-phase, since a function of the availability of extracellular Mg appears to follow an exponential process [33]. Consequently, the extracellular Mg effectively impacts cell physiological behavior; more specifically, the addition of Mg may cause a rapid rise in cell function, such as proliferation and migration.

The enhancement of cellular activity can be achieved via microstructure-modified Mg alloy implantation to acquire a extracellular Mg ion-rich environment. By applying cell viability and wound healing assay, we demonstrated the first report of the promoting effect for wound healing of NIH-3T3 cells using microstructure-modified magnesium alloy to acquire the proper extracellular magnesium concentration. According to the above studies and the results reported here, we logically constructed a reasonable pathway to demonstrate the promoting mechanism of microstructure-modified ZK60 on the wound-healing process (see Fig. 7). Moreover, the

common problem of hydrogen-bubble accumulation (which may cause cutaneous emphysema [8]) can be minimized via proper solid-solution heat treatment, which improves the applicability of ZK60. Both the in vitro corrosion results and biological behavior demonstrate the considerable potential of H400 for application in biodegradable materials (Fig. 8).

4 Conclusion

The uniformity of ZK60 was enhanced using solid-solution heat treatment (H400). The H400 treated matrix was twin-free and homogenous, and thus corrosion could be effectively minimized. Heat treatment modification requires precisely controlled temperature to prevent abnormal grain growth for ZK60 magnesium alloys. The corrosion resistance of a coarse-grained microstructure (H500) is not reliable for degradation processes in biological environments. H400 featured good corrosion resistance and released a affordable concentration of Mg ions (13.2 mM), which can promote the cell viability and wound repair in vitro, confirming its potential for biomedical applications.

References

1. Staiger MP, Pietak AM, Huadmai J, Dias G. Magnesium and its alloys as orthopedic biomaterials: a review. Biomaterials. 2006;27:1728–34.
2. Hornberger H, Virtanen S, Boccaccini AR. Biomedical coatings on magnesium alloys—a review. Acta Biomater. 2012;8:2442–55.
3. Zhang SX, Zhang XN, Zhao CL, Li JA, Song Y, Xie CY, et al. Research on an Mg-Zn alloy as a degradable biomaterial. Acta Biomater. 2010;6:626–40.
4. Li ZJ, Gu XN, Lou SQ, Zheng YF. The development of binary Mg-Ca alloys for use as biodegradable materials within bone. Biomaterials. 2008;29:1329–44.
5. Lin DJ, Hung FY, Lui TS, Yeh ML. Heat treatment mechanism and biodegradable characteristics of ZAX1330 Mg alloy. Materials science & engineering C, Materials for biological applications. 2015;51:300–8.
6. Heublein B, Rohde R, Kaese V, Niemeyer M, Hartung W, Haverich A. Biocorrosion of magnesium alloys: a new principle in cardiovascular implant technology? Heart. 2003;89:651–6.
7. Li X, Chu CL, Liu L, Liu XK, Bai J, Guo C, et al. Biodegradable poly-lactic acid based-composite reinforced unidirectionally with high-strength magnesium alloy wires. Biomaterials. 2015;49:135–44.
8. Kirkland NT, Birbilis N, Staiger MP. Assessing the corrosion of biodegradable magnesium implants: a critical review of current methodologies and their limitations. Acta Biomater. 2012;8:925–36.
9. Zhang WJ, Li MH, Chen Q, Hu WY, Zhang WM, Xin W. Effects of Sr and Sn on microstructure and corrosion resistance of Mg-Zr-Ca magnesium alloy for biomedical applications. Mater Design. 2012;39:379–83.
10. Pu Z, Song GL, Yang S, Outeiro JC, Dillon OW, Puleo DA, et al. Grain refined and basal textured surface produced by burnishing for improved corrosion performance of AZ31B Mg alloy. Corros Sci. 2012;57:192–201.
11. Aung NN, Zhou W. Effect of grain size and twins on corrosion behaviour of AZ31B magnesium alloy. Corros Sci. 2010;52:589–94.
12. Janning C, Willbold E, Vogt C, Nellesen J, Meyer-Lindenberg A, Windhagen H, et al. Magnesium hydroxide temporarily enhancing osteoblast activity and decreasing the osteoclast number in peri-implant bone remodelling. Acta Biomater. 2010;6:1861–8.
13. Sternberg K, Gratz M, Koeck K, Mostertz J, Begunk R, Loebler M, et al. Magnesium used in bioabsorbable stents controls smooth muscle cell proliferation and stimulates endothelial cells in vitro. J Biomed Mater Res B. 2012;100B:41–50.
14. Nguyen TY, Cipriano AF, Guan RG, Zhao ZY, Liu H. In vitro interactions of blood, platelet, and fibroblast with biodegradable magnesium-zinc-strontium alloys. J Biomed Mater Res A. 2015;103(9):2974–86.
15. Hartwig A. Role of magnesium in genomic stability. Mutat Res-Fund Mol M. 2001;475:113–21.
16. Zreiqat H, Howlett CR, Zannettino A, Evans P, Schulze-Tanzil G, Knabe C, et al. Mechanisms of magnesium-stimulated adhesion of osteoblastic cells to commonly used orthopaedic implants. J Biomed Mater Res. 2002;62:175–84.
17. Tapiero H, Tew KD. Trace elements in human physiology and pathology: zinc and metallothioneins. Biomed Pharmacother. 2003;57:399–411.
18. ISO 10993-5 I. Biological evaluation of medical devices. Part 5 Tests for Cytotoxicity: In Vitro MethodsANSI/AAMI, Arlington, VA (1999).
19. Massalski TB. Binary alloy phase diagrams. Ohio: Am Soc Metals; 1986.
20. Song GL. Recent progress in corrosion and protection of magnesium alloys. Adv Eng Mater. 2005;7:563–86.
21. Kannan MB, Raman RKS. In vitro degradation and mechanical integrity of calcium-containing magnesium alloys in modified-simulated body fluid. Biomaterials. 2008;29:2306–14.
22. Stern M, Geary AL. Electrochemical polarization. 1. A theoretical analysis of the shape of polarization curves. J Electrochem Soc. 1957;104:56–63.
23. Zhao MC, Liu M, Song GL, Atrens A. Influence of microstructure on corrosion of as-cast ZE41. Adv Eng Mater. 2008;10:104–11.
24. Mueller WD, Nascimento ML, de Mele MFL. Critical discussion of the results from different corrosion studies of Mg and Mg alloys for biomaterial applications. Acta Biomater. 2010;6:1749–55.
25. Cheng YL, Qin TW, Wang HM, Zhang Z. Comparison of corrosion behaviors of AZ31, AZ91, AM60 and ZK60 magnesium alloys. T Nonferr Metal Soc. 2009;19:517–24.
26. Liu CL, Wang YJ, Zeng RC, Zhang XM, Huang WJ, Chu PK. In vitro corrosion degradation behaviour of Mg-Ca alloy in the presence of albumin. Corros Sci. 2010;52:3341–7.
27. Walker GM, Duffus JH. Magnesium-Ions and the Control of the Cell-Cycle in Yeast. J Cell Sci. 1980;42:329–56.
28. Valerio P, Pereira MM, Goes AM, Leite MF. The effect of ionic products from bioactive glass dissolution on osteoblast proliferation and collagen production. Biomaterials. 2004;25:2941–8.

29. Zhao N, Zhu DH. Endothelial responses of magnesium and other alloying elements in magnesium-based stent materials. Metallomics. 2015;7:113–23.

30. Lange TS, Kirchberg J, Bielinsky AK, Leuker A, Bank I, Ruzicka T, et al. Divalent cations (Mg^{2+}, Ca^{2+}) differentially influence the beta 1 integrin-mediated migration of human fibroblasts and keratinocytes to different extracellular matrix proteins. Exp Dermatol. 1995;4:130–7.

31. Grzesiak JJ, Pierschbacher MD. Changes in the concentrations of extracellular Mg++ and Ca++ down-regulate E-cadherin and up-regulate Alpha(2)Beta(1) integrin function, activating keratinocyte migration on type-I collagen. J Invest Dermatol. 1995; 104:768–74.

32. Rubin H. Magnesium: the missing element in molecular views of cell proliferation control. BioEssays. 2005;27:311–20.

33. Hazelton B, Mitchell B, Tupper J. Calcium, magnesium, and growth-control in the Wi-38 human fibroblast cell. J Cell Biol. 1979;83:487–98.